processes

MDPI

Article

Arsenic Removal from Mining Effluents Using Plant-Mediated, Green-Synthesized Iron Nanoparticles

Pari Karimi [1], Sepideh Javanshir [1,*], Mohammad Hossein Sayadi [2] and Hoda Arabyarmohammadi [3]

1 Mining Engineering Department, Faculty of Engineering, University of Birjand, Birjand 9717434765, Iran; parikarimi@gmail.com
2 Environmental Sciences Department, University of Birjand, Birjand 9717434765, Iran; mh_sayadi@birjand.ac.ir
3 Mineral Processing Group, Mining Engineering Department, Tarbiat Modares University, Tehran 1411713116, Iran; hoda1367@aut.ac.ir
* Correspondence: sjavanshir@birjand.ac.ir

Received: 17 September 2019; Accepted: 14 October 2019; Published: 17 October 2019



Abstract: Arsenic contamination in industrial and mining effluents has always been a serious concern. Recently, nano-sized iron particles have been proven effective in sorptive removal of arsenic, because of their unique surface characteristics. In this study, green synthesis of iron nanoparticles was performed using a mixed extract of two plant species, namely *Prangos ferulacea* and *Teucrium polium*, for the specific purpose of arsenic (III) removal from the aqueous environment. Results of UV-visible spectrometry, X-ray powder diffraction (XRD), and Fourier-transform infrared spectroscopy (FTIR) analyses confirmed the formation of iron nanoparticles from *Prangos ferulacea (Pf)* and *Teucrium polium (Tp)* extracts. The synthesized Fe nanoparticles morphology was studied via microscopy imaging. The particle size was 42 nm, as assessed by dynamic light scattering (DLS) analysis. Adsorption experiments were also designed and performed, which indicated 93.8% arsenic removal from the aqueous solution at 200 rpm agitation rate, 20 min agitation time, pH 6, initial concentration of 0.1 g/L, and adsorbent dosage of 2 g/L. Adsorption isotherm models were investigated, and the maximum uptake capacity was determined to be about 61.7 mg/g. The kinetic data were best represented by the pseudo-second kinetic model (R^2 = 0.99). The negative value of Gibbs free energy, the enthalpy (−7.20 kJ/mol), and the entropy (−57 J/mol·K) revealed the spontaneous and exothermic nature of the adsorption process. Moreover, the small quantity of the activation energy confirmed the physical mechanism of arsenic adsorption onto iron nanoparticles and that the process is not temperature sensitive.

Keywords: arsenic adsorption; isotherm model; process optimization; thermodynamics; kinetics study

1. Introduction

Arsenic is known as a carcinogenic element that may enter # aquatic environments through either natural processes, such as weathering, biological activities, and volcanic emissions, or anthropogenic practices, including mining and metallurgical activities or glass and ceramic manufacture [1]. With an average concentration of 6 mg/kg, arsenic is the twentieth most abundant element within the earth's crust, being present in over 2000 mineral compounds [2]. It may exist in the form of arsenate (60%), arsenite (20%), sulfide, and sulfur-containing salts (20%). Inorganic arsenic in natural waters is usually found in the form of arsenate oxyanions (As (V)) or arsenite (As (III)). Arsenite is 25–60 times more

toxic than arsenate, more mobile in aqueous environments, and more hazardous to the environment. Long-term consumption of arsenic-contaminated water is a threat to human health [3]. Among the chronic effects of exposure to arsenic are the spread of cancers, skin diseases, and infertility. According to World Health Organization (WHO) and United States Environmental Protection Agency (USEPA), the maximum arsenic concentration limit in drinking water is 10 μg/L [4].

Several methods have been proposed for removal of arsenic from aqueous solutions, each having their unique limitations and benefits. The available strategies generally include the oxidation-based [5,6], coagulation, settlement, and filtration methods [7,8]; and membrane [9], ion-exchange [10], and adsorption processes [11,12]. Most arsenic removal methodologies are non-effective for arsenite ions, which are predominantly non-charged at pH < 9.2 [5]. The precipitation, adsorption, and ion-exchange methods are, therefore, less applicable for removal of trivalent arsenic. Accordingly, the optimum arsenic removal methods are usually composed of two individual stages: initial oxidation of arsenite to arsenate, and subsequent removal of arsenate [13].

In spite of the availability of biological and chemical methods (chemical oxidation, electrochemical acidification) to remove arsenic from the aqueous solutions, the efficiency of some natural and agro-based sorbents, such as banana peel [14], rice husk [15], red mud [16], clay minerals [17], and polymeric materials [18], has been investigated. Among the other sorbents tested, metallic nanoparticles, such as titanium, zirconium, and iron, have shown higher sorption efficiencies towards arsenic ions. In recent years, iron nanoparticles (FeNPs) have attracted much attention in the field of organic and inorganic contaminant removal. Successful results have been obtained in the utilization of FeNPs for arsenic decontamination [19].

The fate and contamination of nanoparticles synthesized through chemical processes and their unwanted toxic by-products are of concern. However, through the production of bio-based methods, safe production of nanomaterials has considerably increased. The conventional chemical methods in the fabrication of nanoparticles are being substituted with green chemistry methodology. Unlike physical and chemical methods, this novel method does not rely on high input energy, pressure, temperature, or utilization of chemical reagents.

Among the biological methods, the utilization of plant extracts seems to be more feasible, as the metal ions are mitigated quickly. Nanoparticles are synthesized within a few minutes or hours, considering the plant type and phytochemical concentration, while in microbial methods, considerably longer processing time is required [20]. Therefore, utilization of plants and their derivatives in the fabrication of nanomaterials is prioritized, in which green synthesis of metal nanoparticles is facilitated by using various plant organs, such as leaves, stems, roots, and seeds [21]. Plant-derived polyphenolic and flavonoid compounds, L-ascorbic acid (vitamin C), proteins, caffeine, theophylline, and antioxidants accelerate the synthesis of nanoparticles [22]. Herein, some of the mentioned substances act as reducing agents, while some others act as stabilizers and dispersants [23].

To the best of our knowledge, the plant-mediated synthesis of FeNPs has not been reported with the *Prangos ferulacea* and *Teucrium polium* extracts. This selection was based on the abundance, low-cost, and availability of the corresponding plant species in the area of study, the novelty of their incorporation, and their chemical specifications. The phenolic content of *Prangos ferulacea* and *Teucrium polium* is 65 [24] and 150 mg [25], respectively. These plants act as both reducing and capping agents.

The study aims to prepare iron nanoparticles (FeNPs) using an eco-friendly approach in one step by reduction of $FeSO_4$ with polyphenols from *Prangos ferulacea* and *Teucrium polium*. The resulting product is non-toxic, eco-accommodating, and cost-effective. Hence, it can be used as an economical alternative for FeNP production on a large-scale. Also, the synthesized nanoparticles were fully characterized, and consequently, the sorptive behavior of FeNPs was assessed through equilibrium and kinetic adsorption tests for arsenic removal from mining effluents, which has not yet been reported. Adsorption efficiency was investigated in different experimental conditions and was compared with that of conventional sorbents.

2. Material and Methods

2.1. Synthesis of Iron Nanoparticles

The collected plant samples were thoroughly rinsed with deionized water, air dried, and pulverized. Next, 15 g of plant powder was agitated with 250 mL deionized water for 1 h at 80 °C [26] using a magnetic hotplate stirrer (HSD330, MTops, Gyeonggi-do, Korea). The final extract was filtered using a vacuum pump (PLATINUM, Aurora, IL, USA). Iron sulfate (0.1 M) and sulfuric acid (0.1 M) were added into the solution to minimize and reduce Fe^{2+} oxidation. The extract solution was mixed with 0.1 M iron sulfate solution at a ratio of 2:1, while agitating the mixture for 30 min at room temperature. The nitrogen gas was injected into the mixture because the dissolved oxygen had been removed. Immediately after mixing, the solution changed color from light brown to dark black. This phenomenon is attributed to the formation of iron nanoparticles based on previous studies [20]. The nanoparticles were carefully filtered and dried at 50 °C for 24 h in a vacuum oven.

2.2. Characterization of Iron Nanoparticles

UV-visible spectrometry (Shimadzu UV2550, Kyoto, Japan) detected nanoparticles within 190–700 nm absorbance spectra. Mineral phases in the specimens were detected using X-ray powder diffraction (XRD) analysis (Philips pw1730, Amsterdam, The Netherlands). Field emission scanning electron microscopy (FESEM) (BEL SORP mini, Osaka, Japan), transmission electron microscopy (TEM) under an accelerating voltage of 100 kV (Zeiss EM 10C), and dynamic light scattering (DLS) (ZEN 3600, Malvern, Worcestershire, UK) were applied to study the size and morphology of the material. The surface functional group responsible for reduction, covering, and stabilization of the reduced nanoparticles was identified by interpreting the Fourier-transform infrared spectroscopy (FTIR) spectrum (BRAIC WQF-510, Beijing, China). The pH of zero points of charge (pH_{ZPC}) of the sorbent was estimated by preparing several samples at different pHs and detecting their zeta potentials using a Nano ZS ZEN3600 device (Malvern, Worcestershire, UK).

2.3. Adsorption Experiments

Batch adsorption experiments were designed and performed using 25-mL flasks containing 20 mL aqueous arsenic solution with a dose of adsorbent added, and then agitated by an orbital shaker at room temperature (25 ± 1 °C). According to Table 1, the effects of 5 different parameters on arsenic removal were assessed: pH, time, agitation rate, adsorbent dosage, and initial concentration (test series 1–5, respectively). Factors were changed one at a time, while the others were kept constant. The pH adjustments were made by adding proper amounts of HCl (37%, c) and 0.1 M NaOH (BDH chemicals Co, Hull, UK) to the solution. Samples were withdrawn at predetermined time intervals, filtered, and then analyzed for their arsenic content by AAS (ContrAA700, Jena, Germany). Each experiment was repeated three times, and the mean value was reported. The standard solution was analyzed to achieve stability and accuracy.

The arsenic removal at a time (t) was then calculated according to Equation (1). The amount of arsenic adsorbed at time t, q_t (mg/g), was calculated by Equation (2).

$$Removal\ (\%) = \frac{(C_0 - C_t)}{C_0} * 100 \quad (1)$$

$$q_t = \frac{(C_0 - C_t)V}{W} \quad (2)$$

where C_0 is the initial arsenic concentration, and C_t is the concentration at time (t). V is the volume of the arsenic solution (L), and m is the mass of adsorbent (g).

Test series five was also used to study the equilibrium isotherm model. Table 2 lists the details of the isotherm models and their parameters selected for this study.

Table 1. Summary of the design of adsorption experiments.

	Parameters				
	pH	**Time (min)**	**Agitation Rate (rpm)**	**Adsorbent Dose (g/L)**	**Initial Arsenic Concentration (mg/L)**
Series 1	4, 5, 6, 7, 8,9	15	150	2	75
Series 2	6	5, 15, 20, 40, 60, 80, 100, 120	150	2	75
Series 3	6	20	100, 150, 200, 250	2	75
Series 4	6	20	200	0.5, 1, 1.5, 2, 2.5, 3	75
Series 5	6	20	200	2	25, 50, 75, 100, 150

Table 2. Isotherms and their linearized expressions.

Isotherms	Equations	Linear Expression	Plot	Parameters
Freundlich	$q_e = LnK_F(C_e)^{1/n}$	$lnq_e = LnK_F + \frac{1}{n}lnC_e$	lnq_e *vs.* lnC_e	K_F = exp(intercept) n = (slope)$^{-1}$
Langmuir	$q_e = \frac{(q_m K_L C_e)}{(1+K_L C_e)}$	Type(I) $\frac{C_e}{q_e} = \left(\frac{1}{K_L q_m}\right) + \left(\frac{C_e}{q_m}\right)$	$\left(\frac{C_e}{q_e}\right)$ *vs.* C_e	q_m = (slope)$^{-1}$ K_L = slope/intercept
Temkin	$q_e = q_m \ln(K_T C_e)$	$q_e = q_m lnK_T + q_m lnC_e$	q_e *vs.* lnC_e	q_m = exp (intercept/slope) K_L = slope
Redlich-Peterson	$q_e = \frac{A_{RP}C_e}{1+B_{RP}C_e^g}$	$\ln\left[\left(\frac{A_{RP}C_e}{q_e}\right) - 1\right] = g lnC_e + lnB_{RP}$	$\ln\left[\left(\frac{A_{RP}C_e}{q_e}\right) - 1\right]$ *vs.* lnC_e	G = slope B_{RP} = exp (intercept) A_{RP} *
Koble–Corrigan	$q_e = \frac{A_{KC}C_e^p}{1+B_{KC}C_e^p}$	$\frac{1}{q_e} = \frac{\left(\frac{1}{A_{KC}C_e^p}\right)}{\left(\frac{B_{KC}}{A_{KC}}\right)}$	$\frac{1}{q_e}$ *vs.* $\frac{1}{C_e^p}$	A_{KC} = (slope)$^{-1}$ B_{KC} = intercept/slope P *

Note: * optimized using a trial and error method.

To study the kinetics model, the sorption experiments were performed at an initial arsenic concentration of 75 mg/L, sorbent dosage of 0.04 g/L, pH 6, and agitation rate of 150 rpm. Samples were withdrawn at predetermined time intervals (5, 15, 20, 40, 60, 80, 100, and 120 min) during agitation. The kinetic data were analyzed using well-known kinetic models, as given in Table 3.

Table 3. Kinetic models and their linearized expressions.

Kinetic Model	Equations	Linear Expression	Plot	Parameters
Zero order	$q_t = q_e - k_0 t$	$q_t = q_e - k_0 t$	q_t vs. t	k_0 = −slope q_e = intercept
First order	$q_e = q_t \exp(k_1 t)$	$Ln(q_e/q_t) = k_1 t$	$\ln(q_t)$ vs. t	k_1 = −slope qe = exp (intercept)
Pseudo-first order	$q_t = q_e[1 - \exp(k_{1p} t)]$	$Ln(q_e - q_t) = lnq_e - k_1 t$	$\ln(q_e - q_t)$ *vs.* t	k_1 = −slope qe = exp (intercept)
Pseudo-second order	$q_t = k_{2p} q_e^2 t/(1 + q_e k_{2p} t)$	$\frac{t}{q_t} = \frac{1}{k_{2p} q_e^2} + \frac{t}{q_e}$	$\frac{t}{q_t}$ *vs.* t	k_{2p} = (slope)^2/intercept qe = (slope)$^{-1}$
Elovich	$q_t = \frac{1}{\beta}\ln(\alpha\beta t)$	$q_t = \frac{1}{\beta}\ln(\alpha\beta) + \frac{1}{\beta} lnt$	q_t *vs.* lnt	B = (slope)$^{-1}$ α = (slope) exp (intercept/slope)
Exponential function	$q_t = kt^v$	$Lnq_t = lnk + vlnt$	Lnq_t *vs.* lnt	V = slope K = exp(intercept)

The best-fit isotherm and kinetic models were determined according to the coefficient of determination (R^2 value).

Moreover, to study the thermodynamics of the adsorption, experiments were performed at an initial arsenic concentration of 100 ppm, pH 6, adsorbent dosage of 2 g/L, agitation rate of 200 rpm, and five different temperatures (20, 40, 50, 60, and 70 °C) for 20 min.

3. Results and Discussion

3.1. Characterization of the Synthesized Nanoparticles

As mentioned earlier, the color of the solution changed during nanoparticle formation. The color change in the mixture of extracts after their addition to the iron solution indicates the formation of the nanoparticle [27].

Figure 1 shows the absorption spectra in the case of mixed extracts, iron sulfate, and the synthesized nanoparticles. The spectrum showed a peak at 240 nm, which indicates the presence of Fe(II) ion. The resonance wavelength for iron nanoparticles lies in the range of 400–500 nm. A peak range of 390–450 nm was attributed to the zero-valent iron state, which is in full agreement with the results of other reports using various plants such as goua, papaya, and neem leaf extracts [28].

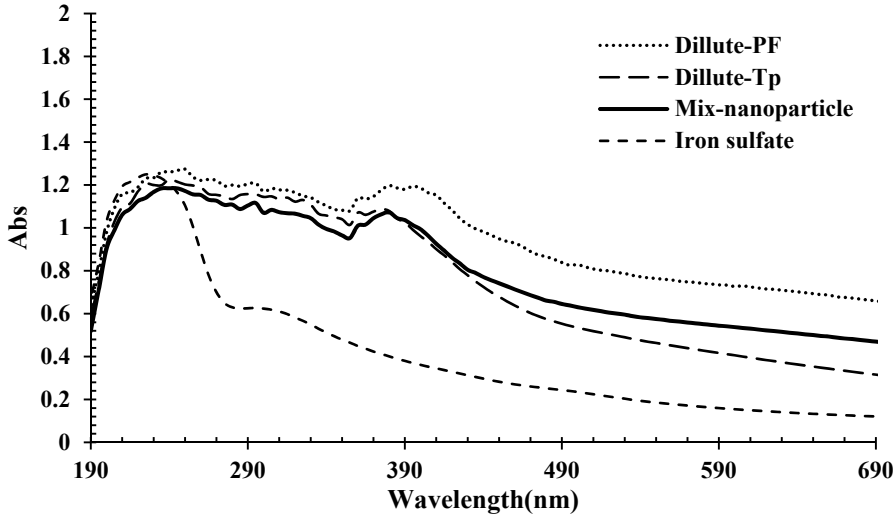


Figure 1. UV-Vis spectra related to the plant extracts, iron solution, and the synthesized nanoparticles.

After 10 min, the reaction was finished, and the peak disappeared, representing the complete reduction of Fe(II) ions to FeNPs. According to the UV-Vis analysis, the presence of the iron nanoparticle was confirmed, and further characterization studies focused on the synthesized FeNPs by mixture of extracts.

The FTIR spectra showed several peaks at different regions, which indicated the biological nature of the iron complexes. In Figure 2a (before the adsorption process), the band at 3407 cm^{-1} was attributed to hydroxyl (OH) groups. The band at 1625 cm^{-1} represented the C=C aromatic ring stretching vibration and confirmed the existence of poly-phenolic compounds (aromatic cycles) in the extracts. The absorption band in the C–H region showed the polyols, and vibrations at 1100 cm^{-1} were attributed to the C–O bond. The peak at 590 cm^{-1} was assigned to the Fe–O bond [29].

Overall, the peaks confirm the presence of protein, phenolic, and amide groups in the extract mixture, which are responsible for the reduction of salt precursors to nanoparticles. Flavonoids are thermodynamically able to reduce the Fe^{2+} to Fe^0 because of their lower redox potential ($0.23 < E < 0.75$ V). Therefore, the Fe–O bond appeared at 590 cm^{-1}, confirming the presence of Fe nanoparticles. Figure 2b shows the shift of peaks at 3407, 2925, 1625, 1100, and 590 cm^{-1} to new positions at 3419, 2900,

1621, 1089, and 572 cm^{-1} (after the adsorption process), respectively. These changes in the vibration peaks indicate the higher sorption intensity, and confirm the arsenic adsorption onto iron nanoparticles.

The mechanism of nanoparticle production via biomolecules is challenging. However, the researchers found that phenolic compounds, such as flavonoids, derived from a plant may control the reduction of ferrous cations, and also act as capping agents [30].

The XRD results (Figure 3) confirmed the crystalline form of produced FeNPs, with the peaks at (2θ) 44.38° and 34.38° corresponding to the zero valent iron (Fe^0) and magnetite (Fe_3O_4), respectively. Also, the detected peak at the 2-Theta of 27.13° is related to iron hydroxide (FeOOH). The polyphenolic compound is observed as a sharp peak at 17.58° [31]. This observation is significant for nanoparticles, which mainly consist of maghemite and hydroxide partially oxidized on their surface.

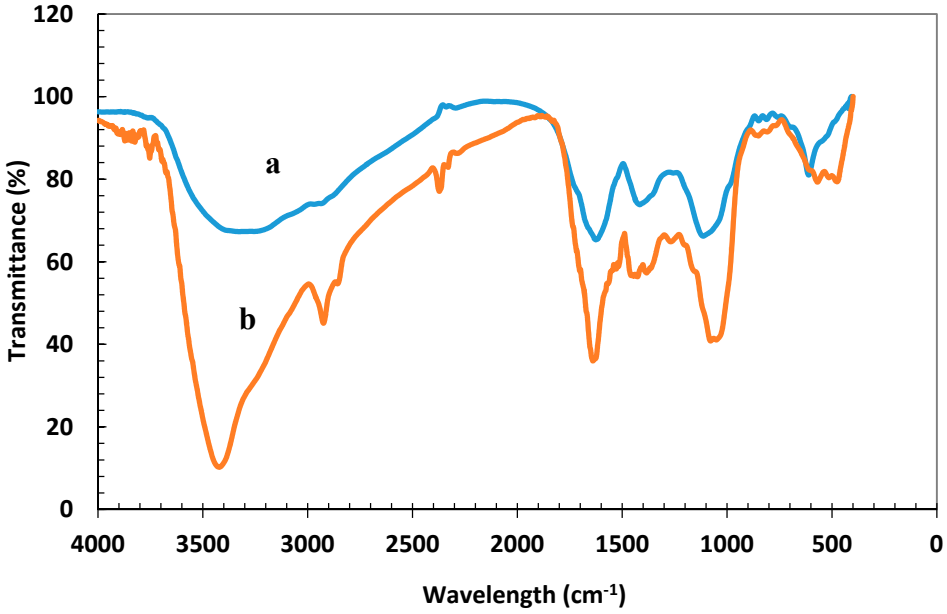


Figure 2. Fourier-transform infrared spectroscopy (FTIR) spectrum of iron nanoparticles (NPs) (**a**) before and (**b**) after the adsorption process (resolution = 4, scan times = 10).

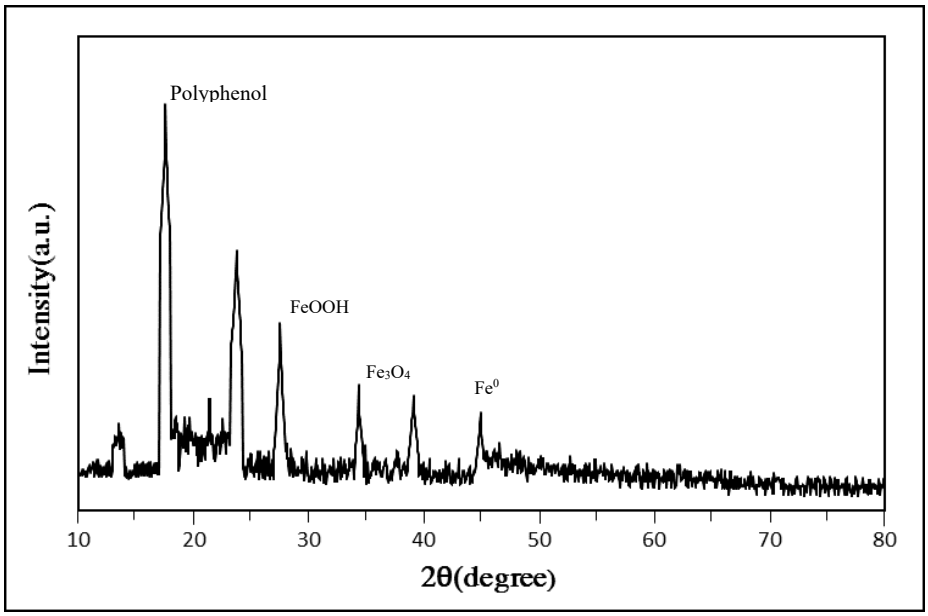


Figure 3. X-ray diffraction (XRD) pattern of synthesized iron nanoparticles from the mixture of extracts.

The morphology and structure of the synthesized nanoparticles were studied using field emission scanning electron microscopy (FESEM). The results of FESEM imaging at two different magnifications of 1 µm and 200 nm are given in Figure 4a. The particles were mostly spherical, with an average size of 30–70 nm. The size range was in agreement with many recent studies (50–100 nm). Okoth et al. reported an average size of 1–2 µm for synthesized iron nanoparticles from banana peel extract [32], while aqueous sorghum bran produced smaller particles (200 nm) [33]. Wang et al. reported that the average size distribution obtained from a mixture of green tea and eucalyptus was about 100 nm [34].

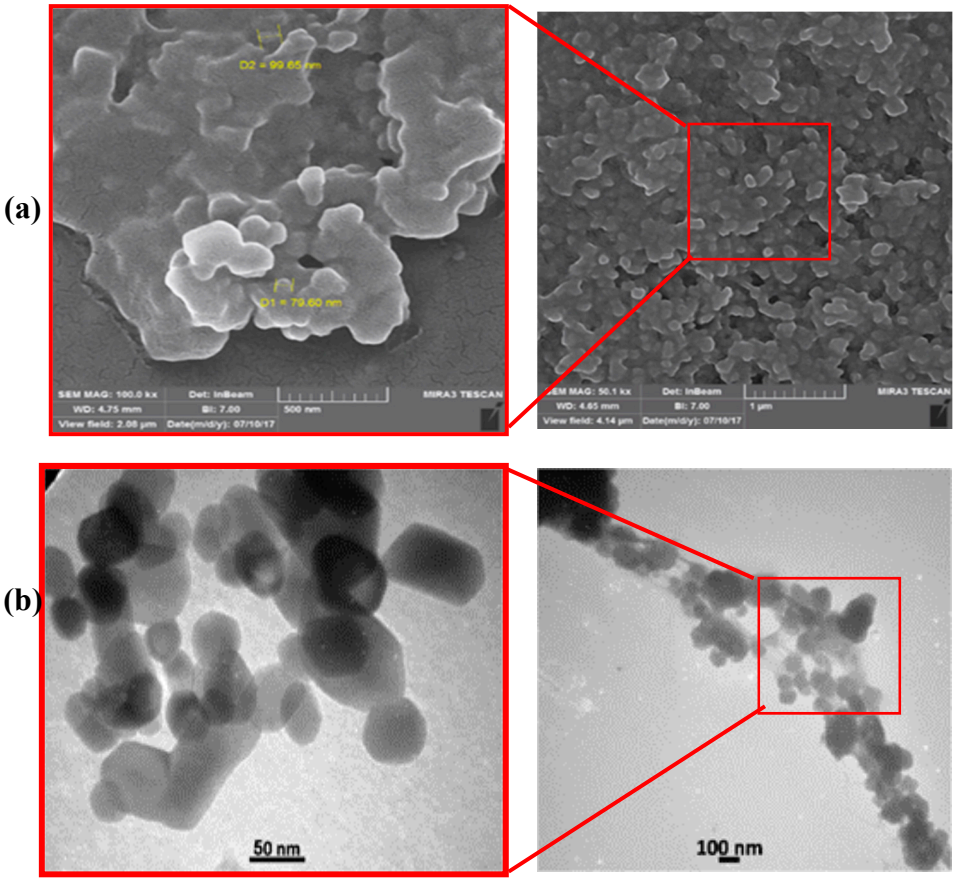


Figure 4. Field emission scanning electron microscopy (FESEM) analysis of synthesized iron nanoparticles at two different magnifications. (**a**) Transmission electron microscopy (TEM) micrograph of iron exposed by a mixture of extracts (**b**).

TEM and SEM analysis demonstrated the surface morphology of biosynthesized FeNPs. The synthesized particles have a uniform spherical structure, with sizes ranging between 35 and 56 nm (Figure 4b). The DLS analysis showed an average particle diameter of 42 nm. It is interesting to note that some of the nanoparticles have irregular shapes because of agglomeration during their preparation for SEM analysis. As a result, most FeNPs were spherical. However, TEM images were compatible with SEM analysis and confirmed the distribution of iron nanoparticle sizes. Similar results using other plant extracts have been reported in the synthesis of $Fe^0/Fe_2O_3/Fe_3O_4$ nanoparticles (Table 4).

Table 4. Size and morphology of $Fe^0/Fe_2O_3/Fe_3O_4$ nanoparticles synthesized by various plant extracts [35].

Plants	Part Used	Size and Morphology
Green tea	Leaf	40–60 nm, Amorphous
Tea	Tea powder	40–50 nm, Spherical
Pomegranate	Leaf	100–200 nm
Azadirachta indica	Leaf	50–100 nm, Spherical
Melaleuca nesophila and *Rosemarinus officinalis*	Leaf	50–80 nm, Spherical
Grapes	Leaf	15–100 nm, Quasi-spherical
Tridax procumbens	Leaf	80–100 nm, Crystalline, irregular sphere shapes
Eucalyptus tereticornis	Leaf	40–60 nm, Cubic

3.2. Optimization of Arsenic Sorption onto Iron Nanoparticles

The influence of the main operating parameters, such as pH, contact time, stirring speed, initial arsenic concentration, adsorbent dosage, and temperature, on arsenic removal from contaminated water was investigated.

The pH plays a role in wastewater treatment processes. Therefore, arsenic removal at different acidity levels was investigated in the range of 4 to 9. Figure 5 illustrates the effects of different initial pHs on arsenic (III) removal efficiency. As can be seen, arsenic removal gradually increased up to pH 6, and then it leveled off, with no further changes for the higher pH values tested. Accordingly, the maximum arsenic removal was found to occur at neutral pH, and therefore, this pH was selected for the rest of the experiments. Low adsorption efficiency at pH 4 was attributed to the competition between As (III) and the protons for the available sorption sites over the sorbent. At pH values higher than 9.2, the negative charge of $H_2AsO_3^-$ leads to electrostatic repulsion [36]. The maximum arsenic removal capacity in the previous studies was also reported at about pH 6–8 [37]. Negative zeta potential at this range of pH confirmed the physical adsorption of arsenic on the adsorbent.

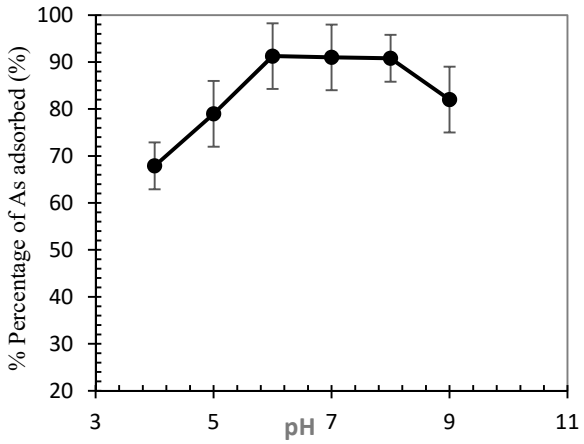


Figure 5. Effect of pH solution on the arsenic removal efficiency (initial arsenic concentration: 0.075 g/L; sorbent dosage: 2 g/L; agitation rate: 150 rpm; time: 15 min).

The effect of contact time on arsenic removal efficiency is illustrated in Figure 6. According to the results, 48.62% of the arsenic was removed during the initial adsorption stage (0–5 min), and as time passed, the arsenic content of the solution decreased at a higher rate so that after 20 min, 93.18% removal was achieved with no specific further change afterward. Thus, to ensure the achievement of equilibrium, the contact time was fixed at 20 min for the rest of the batch experiments. Generally, the rate of adsorption was high at first, and then it experienced a gradual increase until the equilibrium

occurred. This fact may relate to a large number of the vacant surface site at an initial stage, and after a few minutes, the occupation of the rest is difficult due to repulsive forces between the solute molecules in solid and bulk phases [38].

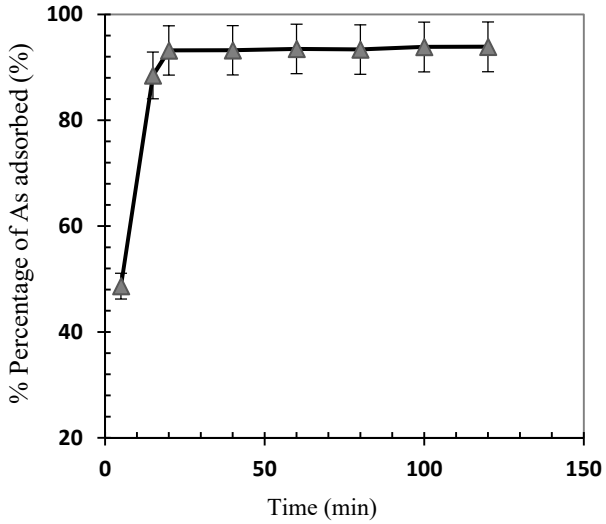


Figure 6. Effect of contact time on arsenic removal efficiency (initial arsenic concentration: 0.075 g/L, sorbent dosage: 2 g/L, agitation rate: 150 rpm, pH = 6).

The agitation rate influences the solute distribution bulk and the thickness of the Nernst boundary film. As can be seen in Figure 7, arsenic uptake increased as the agitation rate was raised to 200 rpm because of lower boundary-layer resistance. Similar results were reported by many researchers [38]. The negative effect of higher stirring speed on adsorption (250 rpm) can be attributed to excessive turbulence of the solution.

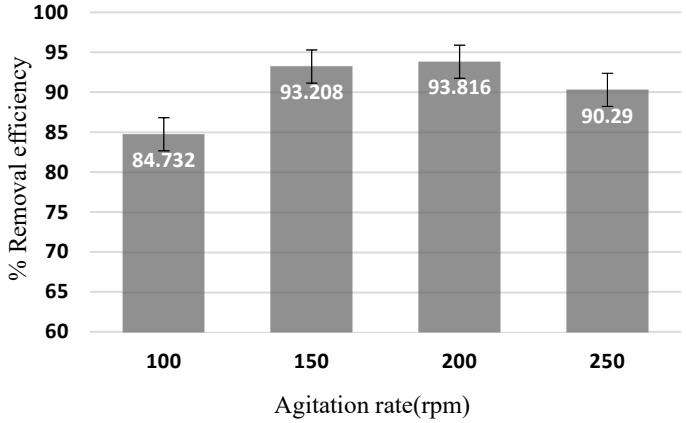


Figure 7. Effect of agitation rate variation on arsenic removal efficiency (initial arsenic concentration: 0.075 g/L, sorbent dosage: 2 g/L, contact time: 20 min, pH = 6).

The effect of adsorbent dosage on removal efficiency was shown in Figure 8. The efficiency of As adsorption considerably increased with the increase of the amount of adsorbent as the maximum static uptake of arsenic (about 93.8%) was achieved for an adsorbent-to-solute ratio of 2 g/L. The reason may be attributed to the fact that the exchangeable sites or surface area are more available for the solute at the higher dosage of the adsorbent [39]. However, a further increase in adsorbent dosage (>2.0 g/L) did not affect the As adsorption due to the completion of adsorption of all arsenic. Thus, 2.0 g/L of iron nanoparticle in contaminated water was chosen for further experiments. The results of this section are in agreement with previous findings by Bazrafshan et al. [40] and Yao et al. [39].

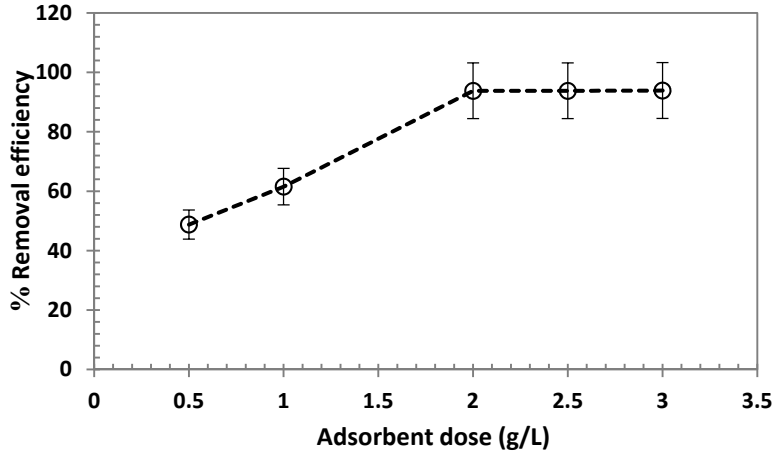


Figure 8. Effect of adsorbent dosage on arsenic removal efficiency (initial arsenic concentration: 0.075 g/L, contact time: 20 min, agitation rate: 150 rpm, pH = 6).

Moreover, Figure 9 illustrates the effect of an initial arsenic concentration on removal efficiency. At an initial concentration of 25 mg/L, 99.92% arsenic removal is achieved by increasing the initial arsenic content, the efficiency is substantially decreased to 64.72%. This may be due to the less availability of the exchangeable sites or mitigation of nanoparticles effective surface area for arsenic capture at higher adsorbate concentration. The maximum capacity of iron nanoparticle for arsenic adsorption was achieved about 61.7 mg/g, which is considerable regarding adsorbent.

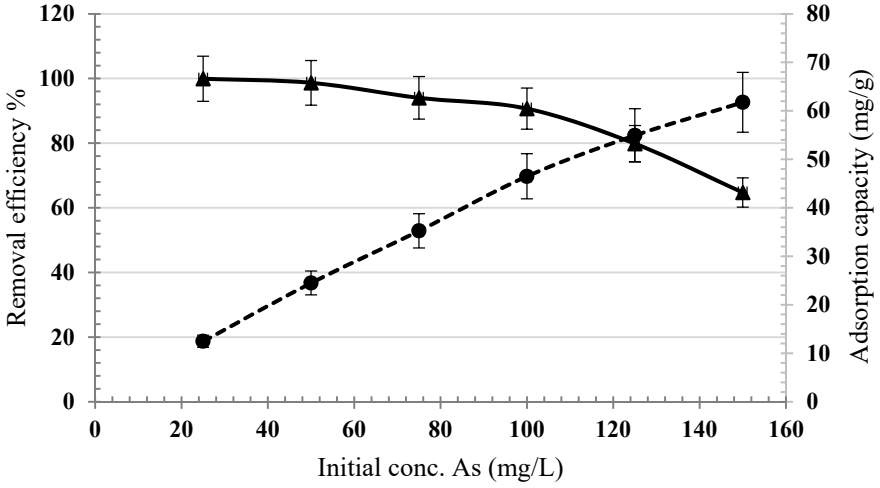


Figure 9. Effect of initial arsenic concentration on arsenic removal efficiency (sorbent dosage: 2 g/L, contact time: 20 min, agitation rate: 150 rpm, pH = 6).

3.3. Arsenic Adsorption Isotherm

The process of adsorption is generally studied through adsorption isotherm curve. This graph shows the distribution of molecules between liquid and solid phase at the equilibrium state, which is considered as a fundamental factor in determining the sorption capacity [41]. To assess the sorption behavior of the iron nanoparticles, some well-known isotherms, namely Langmuir, Fruendlich, Temkin, Redlich–Peterson, and Koble–Corrigan, were considered to describe the phenomena. The results of As adsorption on adsorbents were analyzed by using the linear form of the models. The parameters associated with the adsorption behavior were calculated from the slope, and intercept of the plot. In each isotherm, adsorption capacity increased by raising the equilibrium concentration of arsenic. Isotherms models and their linearized expressions for the arsenic sorption are given in Table 5. The results of adsorption isotherms showed that there exist high correlation coefficients between the

isotherms and experimental data. By comparing the coefficient values, the Redlich-Peterson isotherm had the highest correlation coefficient (R^2 = 0.9987), although only slightly (Figure 10).

Table 5. Arsenic adsorption modeling through different isotherms and their respective parameters.

Isotherms	Parameters	R^2
Freundlich	K_F = 25.81 mg g^{-1} (L mg^{-1})$^{1/n}$ n = 3.75	0.9901
Langmuir	q_m = 64.51 mg g^{-1} K_L = 0.49 L mg^{-1}	0.9849
Temkin	q_m = 8.0041 mg g^{-1} K_L = 45.02 L mg^{-1}	0.917
Redlich-Peterson	g = 1.361 B_{RP} = 32.52 (L mg^{-1}) A_{RP} = 2 mg g^{-1} (L mg^{-1})	0.9987
Koble–Corrigan	A_{KC} = 0.052 mg g^{-1} (L mg^{-1}) B_{KC} = 0.012 (L mg^{-1})^P P = 0.2	0.9974

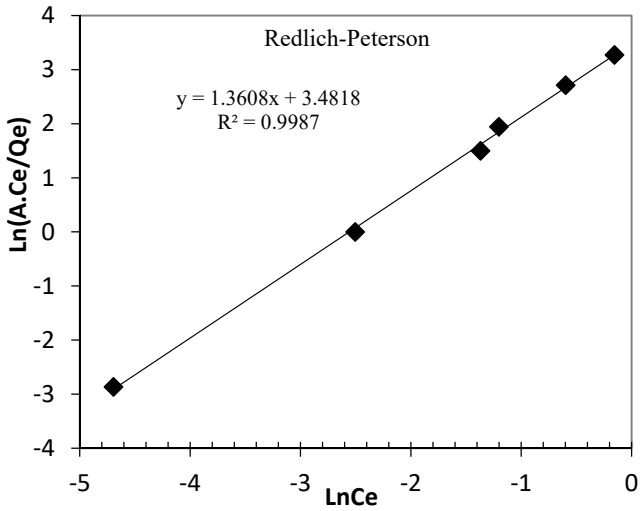


Figure 10. The linearized Redlich–Peterson isotherm model for arsenic sorption onto iron nanoparticles.

3.4. Adsorption Kinetics

By understanding the kinetic sorption model, the mechanisms of the adsorption process are determined, such as mass transfer or chemical reaction. Several kinetic models, such as zero-order, first-order, second-order, pseudo second-order, Elovich, and exponential functions, were used to test the experimental data. The kinetic models, their linear expression form, and the model parameters are summarized in Table 3. The correlation coefficient (R^2) was used for the evaluation of the best kinetic model (Table 6). Among all models, the pseudo-second order kinetic model had a good correlation coefficient, and it fit best with experimental data (Figure 11).

Table 6. Kinetic parameters for arsenic removal using synthesized iron nanoparticles.

Isotherms	Parameters	R^2
Zero-order	K_{0} = −0.0731 mg/g h qe = 41.784 mg/g	0.29
First-order	K_1 = −0.00181/h qe = 41.09 mg/g	0.28
Pseudo-first-order	K_1 = 0.003 1/h qe = 18.81 mg/g	0.32
Pseudo-second-order	K_2 = 0.017 g/mg h qe = 48.87 mg/g	0.99
Elovich	β = 0.24 g/mg α = 478.1 mg/g h	0.63
Exponential function	V = 0.1031 K = 31.31 mg/g h	0.61

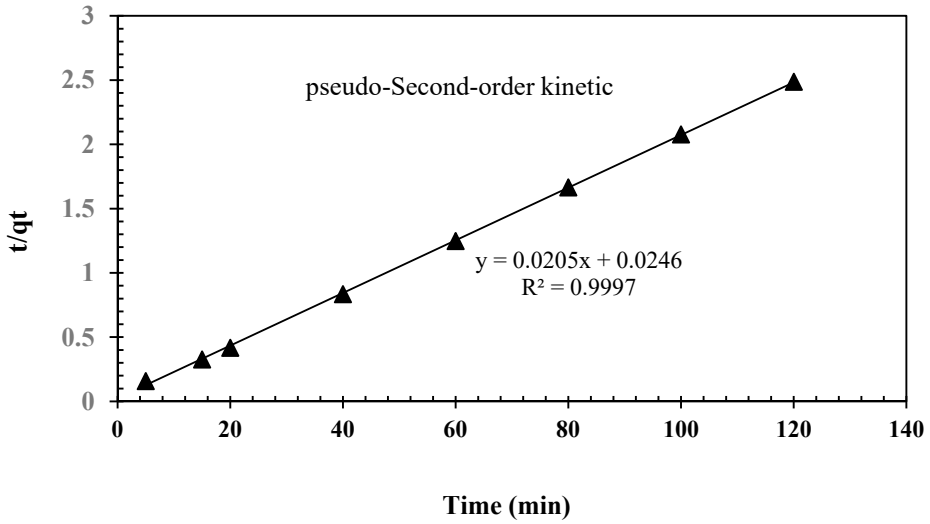


Figure 11. The pseudo-second-order kinetic model for arsenic removal using synthesized iron nanoparticles.

3.5. Thermodynamic Studies

Thermodynamic parameters, such as Gibbs energy (Δ*G*), enthalpy (Δ*H*), and entropy (Δ*S*), may assist in the determination of the possibility, spontaneity, or exothermic or endothermic states of a reaction, which are the critical aspects of an adsorption process. To calculate the thermodynamic parameters, some experiments were carried out at various temperatures ranging 20–70 °C. The amount of arsenic uptake from the solution was decreased from 90% to 73%, respectively (Figure 12). Enthalpy and entropy values were calculated according to the van't Hoff equation:

$$lnk_d = -\left(\frac{\Delta H}{RT}\right) + \left(\frac{\Delta S}{R}\right) \quad (3)$$

where Δ*H* and Δ*S* are the changes in enthalpy and entropy of the adsorption process, respectively. *T* is the temperature (°K), and k_d is the distribution coefficient, which can be calculated by:

$$K_d = (C_0 - Ce)V/CeM \quad (4)$$

where C_0 and C_e are the initial and equilibrium arsenic concentrations, respectively. *V* is the solution volume and *M* is the mass of the adsorbent. By using the van't Hoff equation and plotting lnK_d against

1/*T*, the values of Δ*H* and Δ*S* may be estimated through the slope and intercept of the curve (Figure 11). Moreover, Equation (5) was used to calculate the Gibbs free energy (Δ*G*).

$$\Delta G = \Delta H - T\Delta S \quad (5)$$

The calculated values of the thermodynamic parameters for the arsenic sorption process are listed in Table 7. The negative Δ*H* value indicates the exothermic nature of arsenic sorption onto iron nanoparticles and that the lower temperature favors the reaction (Figure 13). The negative Δ*S* value also shows the adsorption of arsenic ions from the solution onto the iron nanoparticle. Finally, the negative Δ*G* confirms the spontaneous nature of the adsorption and exergonic reaction at all applied temperatures.

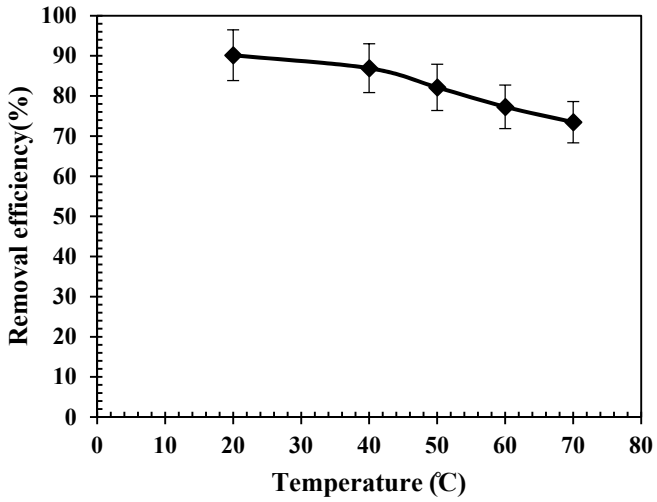


Figure 12. Effect of temperature on arsenic removal efficiency.

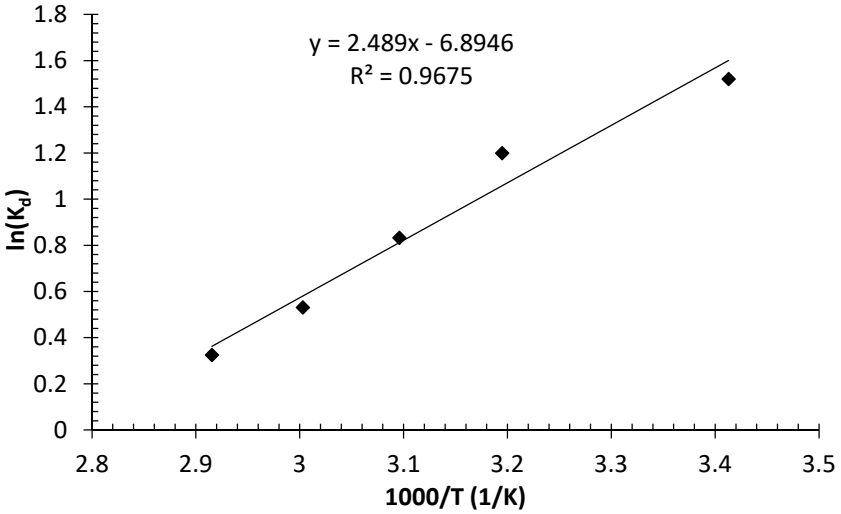


Figure 13. The van't Hoff plot for adsorption of arsenic onto iron nanoparticles.

Table 7. Thermodynamic parameters of arsenic adsorption onto the synthesized iron nanoparticles.

Adsorbent	Initial Concentration (mg/L)	Δ*H* (kJ/mol)	Δ*S* (J/mol·k)	T (°K)	Δ*G* (kJ/mol)
Iron nanoparticles	100	−20.7	−57.3	293	−3898.3
				313	−2751.9
				323	−2178.6
				333	−1605.4
				343	−1032.2

3.6. The Activation Energy of Adsorption

For the evaluation of activation energy, some experiments were performed at the initial arsenic concentration of 100 mg/L and at three different temperatures, 20, 40, and 60 °C. Samples were taken at predetermined time intervals (5, 10, and 20 min) and analyzed for arsenic content by the authors. Figure 14 shows the kinetics of arsenic adsorption onto iron nanoparticles during 20 min of contact time. As can be seen, higher temperatures declined the sorption rate. The activation energy is calculated by the Arrhenieus equation:

$$lnk_l = lnA - \left(\frac{E_a}{RT}\right) \quad (6)$$

where k_l is the pseudo-second kinetic constant, which can be calculated from Figure 12, A is a temperature-independent coefficient (min. g^{-1}. mm^{-1}), E_a is the activation energy (kJ·mol^{-1}), R is the universal gas constant, and T is the temperature (°K).

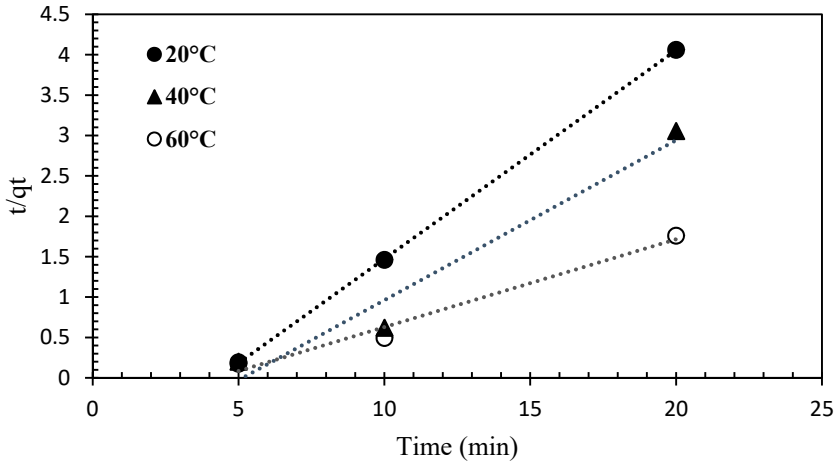


Figure 14. Kinetics of arsenic adsorption at three different temperatures.

E_a can be geometrically estimated by plotting the variations of lnk_l against 1000/T (Figure 15). According to Figure 16, the E_a for the arsenic sorption process is obtained as −17 kJ/mol. This negligible amount of E_a indicates the physical nature of the adsorption process. Therefore, the reaction is not temperature-sensitive, which confirmed that the system was controlled by the diffusion process [42].

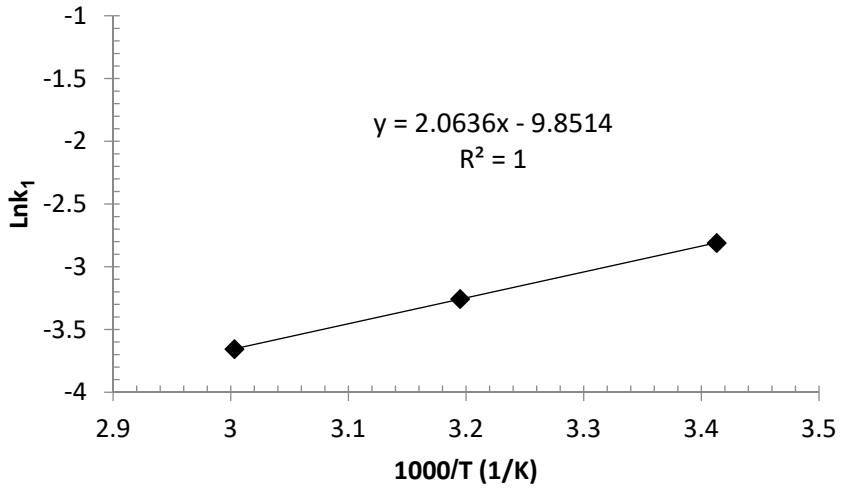


Figure 15. The lnk_1 variations versus 1000/T.

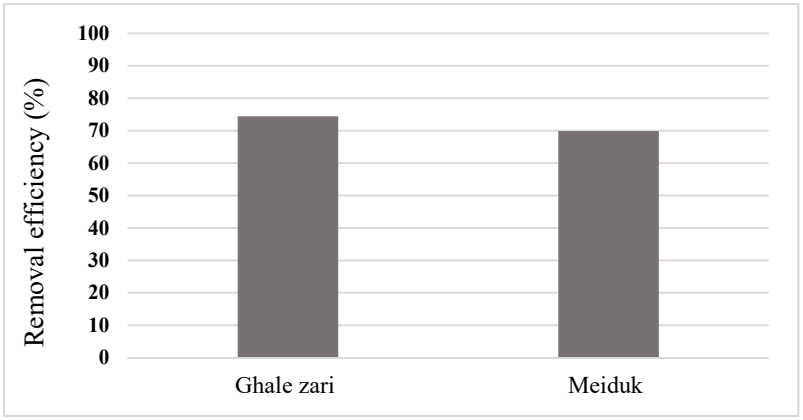


Figure 16. Arsenic removal from industrial mining effluents by synthesized FeNPs.

3.7. Arsenic Removal from Real Mining *Effluents*

Real arsenic-containing effluent samples were collected from Meiduk (Kerman province, Iran) and Ghale Zari (South Khorasan province, Iran) copper processing plants and analyzed for their arsenic contents. The arsenic concentration was 69 µg/L and 43 µg/L for Meiduk and Ghale Zari samples, respectively.

For each sample, an adsorption experiment was performed using 0.04 g adsorbent dosage at optimum conditions, according to the previous tests (pH 6, agitation rate of 200 rpm, 20 min contact time) at ambient temperature. Figure 16 demonstrates the arsenic removal efficiencies in two cases. As can be seen, more than 70% of arsenic can be removed by iron nanoparticles in both cases. Therefore, the adsorbent was successfully confirmed as an efficient option to be considered for mine wastewater treatment plants.

3.8. Comparison of Arsenic Sorption Capacity for Different Adsorbents

Table 8 draws a comparison with the synthesized iron nanoparticles and other reported adsorbents in terms of arsenic adsorption capacity (mg/g). As can be seen, the proposed sorbent is 20 times higher than activated carbon and alumina, which are the conventional materials for arsenic removal. Iron nanoparticles synthesized by *Prangos ferulacea* and *Teucrium polium* leaf extracts still demonstrate a remarkable uptake capacity and may be a promising arsenic removal option to be used in various industrial applications. Note that the other iron-based nano adsorbents, which are illustrated in Table 8, are all chemically produced.

Table 8. The comparison of arsenic sorption capacity for different adsorbents.

No.	Adsorbent	Uptake Capacity (mg/g)	Ref.
1	Granular ferric hydroxide (GFH)	1.1	[43]
2	a-FeOOH nanoparticles	76	[43]
3	Ultra-fine δ-FeOOH	37.3	[43]
4	Hematite	0.2	[44]
5	Magnetite–maghemite nanoparticles	3.71	[43]
6	Red mud	0.94	[44]
7	Fe_3O_4 nanoparticles	46.06	[43]
8	Alumina	25	[43]
9	Activated carbon	3.15	[43]
10	γ-Fe_2O_3 nanoparticles	2.9	[43]
11	Fe_3O_4–γ-Fe_2O_3 nanoparticles	3.71	[43]
12	Nano zero valent iron (NZVI)	1.8–2.0	[43]
13	NZVI/montmorillonite	59.9	[43]
14	Fe–Al layered double hydroxide	40.6	[43]
15	Nano-iron/oyster shell	0.9	[43]
16	NZVI-synthetized by mint	86.53	[44]
17	Iron oxide coated fungal biomass	5.4	[43]
18	Modified iron oxide	0.73	[44]
19	PVA–alginate-supported iron oxide nanoparticles (*IONPs*)	40.3	[35]
20	chitosan-alginate-supported IONPs	34.4	[35]
21	Iron nano particle/Pf-Tp	61.7	Present study

4. Conclusions

Arsenic is one of the toxic and dangerous pollutants in the industrial and mineral processing of wastewater. The purpose of this study is to synthesize biological nanoparticles using the extracts of *Prangos ferulacea* and *Teucrium polium* herbs, and consequently, the application of produced FeNPs for arsenic (III) removal from aqueous solutions. The results of this study can be drawn as follows:

- Iron nanoparticles were synthesized via green chemistry methods. XRD, UV-Vis, and FTIR analyses confirmed the successful formation of iron nanoparticles using *Prangos ferulacea* and *Teucrium polium* leaf extracts, and the morphology was determined as spherical particles of average 40 nm diameter by SEM and TEM analysis.
- The influence of parameters such as contact time, pH, adsorbent dosage, initial arsenic concentration, temperature, and agitation rate was investigated. Results showed that 93.9% of arsenic was eliminated at a stirring speed of 200 rpm, pH 6, 2 g/L nanoparticle dosage, and initial concentration of 0.075 g/L within 20 min.
- The synthesized nanoparticles were able to absorb 61.7 mg/g arsenic from the solution at 298 °K, which is a considerable capacity in comparison with most of the available sorbents. This was also confirmed through post-sorption FTIR analysis.
- The adsorption behavior of the synthesized nanoparticles is represented by different isotherm models.
- Thermodynamic adsorption investigations showed the negative values for enthalpy and entropy of the adsorption process, which revealed its exothermic and spontaneous nature. Moreover, the activation energy for arsenic removal was obtained as −17 kJ/mol, which indicated the physical sorption mechanism and that the process is not temperature-sensitive.
- Arsenic adsorption tests performed over the real industrial effluent samples collected from two different mines confirmed that the proposed adsorbent is capable of removing more than 70% of arsenic contamination in real cases.
- The comparison of arsenic sorption capacity shows that iron nanoparticles synthesized by *Prangos ferulacea* and *Teucrium polium* leaf extracts still demonstrate a remarkable uptake capacity and may be a promising arsenic removal option to be used in various industrial applications.

Author Contributions: Data curation, S.J. and H.A.; Formal analysis, S.J.; Funding acquisition, M.H.S.; Investigation, P.K., S.J., M.H.S. and H.A.; Methodology, S.J. and M.H.S.; Project administration, S.J. and M.H.S.; Resources, S.J. and H.A.; Software, H.A.; Supervision, S.J.; Validation, S.J.; Visualization, P.K.; Writing—original draft, P.K.; Writing—review & editing, S.J., M.H.S. and H.A.

Funding: This research received no external funding.

Acknowledgments: The paper is from a postgraduate student thesis in the Department of Mineral processing, Faculty of Engineering, University of Birjand. Thereby authors appreciate of assistance Laboratories in Natural Resources and Environment at the University of Birjand for conducting some experiments, as well as analysis.

Conflicts of Interest: The authors declare no conflict of interest.

References

1. Tyrovola, K.; Nikolaidis, N.P.; Veranis, N.; Kallithrakas-Kontos, N.; Koulouridakis, P.E. Arsenic removal from geothermal waters with zero-valent iron-Effect of temperature, phosphate and nitrate. *Water Res.* **2006**, *40*, 2375–2386. [CrossRef] [PubMed]
2. Solgi, E.; Esmaili-Sari, A.; Bakhtiari, A.R.R.; Hadipour, M. Soil Contamination by Arsenic in Urban Areas: A case study of Arak City. *Iran. J. Health Environ.* **2015**, *8*, 1–10.
3. Sayadi, M.H.; Rezaei, A.; Sayyed, M.R.G. Grain size fraction of heavy metals in soil and their relationship with land use. *Proc. Int. Acad. Ecol. Environ. Sci. USA* **2017**, *7*, 1–11.
4. World Health Organization. *Arsenic in Drinking Water, Background Document for Preparation of WHO Guidelines for Drinking Water Quality*; World Health Organization: Geneva, Switzerland, 2003.
5. Wei, B.; Yang, L. A review of heavy metal contaminations in urban soils, urban road dusts and agricultural soils from China. *Microchem. J.* **2010**, *94*, 99–107. [CrossRef]
6. Garelick, H.; Dybowska, A.; Valsami-Jones, E.; Priest, N. Remediation Technologies for Arsenic Contaminated Drinking Waters (9 pp). *J. Soils Sediments* **2005**, *5*, 182–190. [CrossRef]
7. Cui, J.; Jing, C.; Che, D.; Zhang, J.; Duan, S. Groundwater arsenic removal by coagulation using ferric(III) sulfate and polyferric sulfate: A comparative and mechanistic study. *J. Environ. Sci.* **2015**, *32*, 42–53. [CrossRef]
8. Shih, M.C. An overview of arsenic removal by pressure-drivenmembrane processes. *Desalination* **2005**, *172*, 85–97. [CrossRef]
9. Molgora, C.C.; Dominguez, A.M.; Avila, E.M.; Drogui, P.; Buelna, G. Removal of arsenic from drinking water: A comparative study between electrocoagulation-microfiltration and chemical coagulation-microfiltration processes. *Sep. Purif. Technol.* **2013**, *118*, 645–651. [CrossRef]
10. Azhdarpoor, A.; Nikmanesh, R.; Samaei, M.R. Removal of arsenic from aqueous solutions using waste iron columns inoculated with iron bacteria. *Environ. Technol.* **2015**, *36*, 2525–2531. [CrossRef]
11. Sayadi, M.H.; Shekari, H. Biosorption of cadmium and lead from aqueous solutions using Spirogyra. *Environ. Stud.* **2017**, *43*, 379–390. [CrossRef]
12. Iravani, S. Green synthesis of metal nanoparticles using plants. *Green Chem.* **2011**, *13*, 2638–2650. [CrossRef]
13. Memon, S.; Bhanger, M.; Memon, J.U.R. Evaluation of banana peel for treatment of arsenic contaminated water. In Proceedings of the 1st Technical Meeting of Muslim Water Researchers Cooperation (MUWAREC), Kuala Lumpur, Malaysia, 15–16 December 2008; pp. 104–109.
14. Asif, Z.; Chen, Z. Removal of arsenic from drinking water using rice husk. *Appl. Water Sci.* **2017**, *7*, 1449–1458. [CrossRef]
15. Altundoğan, H.S.; Altundoğan, S.; Tümen, F.; Bildik, M. Arsenic adsorption from aqueous solutions by activated red mud. *Waste Manag.* **2002**, *22*, 357–363. [CrossRef]
16. Mohammadiazar, S.; Maham, M.; Hasanli, F. Corn-like stationary phase for solid phase microextraction prepared by electro-assisted deposition of sol-gel/silica nanoparticles composite. *Microchem. J.* **2019**, *147*, 914–920. [CrossRef]
17. Rahim, M.; Haris, M.R.H.M. Application of biopolymer composites in arsenic removal from aqueous medium: A review. *J. Radiat. Res. Appl. Sci.* **2015**, *8*, 255–263. [CrossRef]
18. Habuda-Stanic, M.; Stjepanovic, M.N. Arsenic removal by nanoparticles: A review. *Environ. Sci. Pollut. Res.* **2015**, *22*, 8094–8123. [CrossRef]

19. Herlekar, M.; Barve, S.; Kumar, R. Plant-Mediated Green Synthesis of Iron Nanoparticles. *J. Nanopart. Res.* **2014**, *2014*, 9. [CrossRef]
20. Arsiya, F.; Sayadi, M.H.; Sobhani, S. Green synthesis of palladium nanoparticles using Chlorella vulgaris. *Mater. Lett.* **2017**, *186*, 113–115. [CrossRef]
21. Shekari, H.; Sayadi, M.H.; Rezaei, M.R.; Allahresani, A. Synthesis of nickel ferrite/titanium oxide magnetic nanocomposite and its use to remove hexavalent chromium from aqueous solutions. *Surf. Interfaces* **2017**, *8*, 199–205. [CrossRef]
22. Dashora, A.; Sharma, K. Green Synthesis of Nanoparticles and Their Applications. *Adv. Sci. Eng.* **2018**, *10*, 523–541. [CrossRef]
23. Azarkish, P.; Moghadem, M.; Khakdan, F.; Pirbalooti, Y. Variability in morphological traits, total phenolic contents and antioxidant activity in different populations from three species of Prangos from Fars, Kohklouye and Boyerahmad provinces. *EJMP* **2018**, *6*, 20.
24. Stankovic, M.; Martinovic, N.; Mihailovic, V.; Marina, T.; Slavica, S. Antioxidant activity, total phenolic content and flavonoid concentrations of different plant parts of *Teucrium polium* L. Subsp. polium. *Acta Soc. Bot. Pol.* **2012**, *81*, 5. [CrossRef]
25. Peternela, J.; Silva, M.F.; Vieira, M.F.; Bergamasco, R.; Vieira, A.M.S. Synthesis and Impregnation of Copper Oxide Nanoparticles on Activated Carbon through Green Synthesis for Water Pollutant Removal. *Mater. Res.* **2018**, *21*, 11. [CrossRef]
26. Sayadi, M.H.; Salmani, N.; Heidari, A.; Rezaei, M.R. Bio-synthesis of palladium nanoparticle using Spirulina platensis alga extract and its application as adsorbent. *Surf. Interfaces* **2018**, *10*, 136–143. [CrossRef]
27. Latha, N.; Gowri, M. Bio Synthesis and Characterisation of Fe3o4 nanoparticles using Caricaya papaya leaves extract. *Int. J. Sci. Res.* **2014**, *3*, 1551–1556.
28. Ali, I.; Al-Othman, Z.A.; Alwarthan, A. Green synthesis of functionalized iron nano particles and molecular liquid phase adsorption of ametryn from water. *J. Mol. Liq.* **2016**, *221*, 1168–1174. [CrossRef]
29. Chen, Z.; Luo, F.; Yang, D.; Mallavarapu, M.; Naidu, R. Biomolecules in grape leaf extract involved in one-step synthesis of iron-based nanoparticles. *RSC Adv.* **2014**, *4*, 53467–53474.
30. Shahwan, T.; Sirriah, S.A.; Nairat, M.; Boyacı, E.; Eroğlu, A.E.; Scott, T.B.; Hallam, K.R. Green synthesis of iron nanoparticles and their application as a Fenton-like catalyst for the degradation of aqueous cationic and anionic dyes. *Chem. Eng. J.* **2011**, *172*, 258–266. [CrossRef]
31. Okoth, O.J.K. Synthesis and Characterization of Iron Nanoparticles Using Banana Peels Extracts and their Application in Aptasensor. Ph.D. Thesis, University of Nairobi, Nairobi, Kenya, November 2016.
32. Njagi, E.; Huang, H.; Stafford, L.; Genuino, H.; Galindo, H.M.; Collins, J.B.; Hoag, G.; Suib, S. Biosynthesis of Iron and Silver Nanoparticles at Room Temperature Using Aqueous Sorghum Bran Extracts. *Langmuir* **2011**, *27*, 264–271. [CrossRef]
33. Wang, T.; Jin, X.; Chen, Z.; Megharaj, M.; Naidu, R. Green synthesis of Fe nanoparticles using eucalyptus leaf extracts for treatment of eutrophic wastewater. *Sci. Total Environ.* **2014**, *466*, 210–213. [CrossRef]
34. Saif, S.; Tahir, A.; Chen, Y. Green Synthesis of Iron Nanoparticles and Their Environmental Applications and Implications. *Nanomaterials* **2016**, *6*, 209. [CrossRef] [PubMed]
35. Tandon, P.K.; Shukla, R.C.; Singh, S.B. Removal of Arsenic (III) from Water with Clay-Supported Zerovalent Iron Nanoparticles Synthesized with the Help of Tea Liquor. *Ind. Eng. Chem. Res.* **2013**, *52*, 10052–10058. [CrossRef]
36. Chiban, M.; Zerbet, M.; Carja, G.; Sinan, F. Application of low-cost adsorbents for arsenic removal: A review. *J. Environ. Chem. Ecotoxicol.* **2012**, *4*, 91–102.
37. Johnston, R.; Heijnen, H. Safe Water Technology for Arsenic Removal. Technologies for Arsenic Removal from Drink-ing Water, Bangladesh University of Engineering and Technology, Dhaka, Bangladesh. 2001. Available online: https://www.google.com.tw/url?sa=t&rct=j&q=&esrc=s&source=web&cd=3&ved=2ahUKEwiQtsqJ0aLlAhWv3mEKHS1lAh0QFjACegQIAhAC&url=http%3A%2F%2Farchive.unu.edu%2Fenv%2FArsenic%2FHan.pdf&usg=AOvVaw0vhEva1YqNNvNGVO-wCfJB (accessed on 17 September 2019).
38. Bazrafshan, E.; Faridi, H.; Mostafapour, F.K.; Mahvi, A. Removal of Arsenic from Aqueous Environments Using Moringa peregrina Seed Extract as a Natural Coagulant. *Asian J. Chem.* **2013**, *25*, 5. [CrossRef]
39. Yao, S.; Liu, Z.; Shi, Z. Arsenic removal from aqueous solutions by adsorption onto iron oxide/activated carbon magnetic composite. *J. Environ. Health Sci. Eng.* **2014**, *12*, 58. [CrossRef]

40. Khaled, A.; Nemr, A.E.; El-Sikaily, A.; Abdelwahab, O. Removal of Direct N Blue-106 from artificial textile dye effluent using activated carbon from orange peel: Adsorption isotherm and kinetic studies. *J. Hazard. Mater.* **2009**, *165*, 100–110. [CrossRef]
41. Padmavathy, V. Biosorption of nickel (II) ions by baker's yeast: Kinetic, thermodynamic and desorption studies. *Bioresour. Technol.* **2008**, *99*, 3100–3109. [CrossRef]
42. Hao, L.; Liu, M.; Wang, N.; Li, G. A critical review on arsenic removal from water using iron-based adsorbent. *RSC Adv.* **2018**, *8*, 39545–39560. [CrossRef]
43. Shafique, U.; Ijaz, A.; Salman, M.; Zaman, W.U.; Jamil, N.; Rehman, R.; Javaid, A. Removal of arsenic from water using pine leaves. *J. Taiwan Inst. Chem Eng.* **2012**, *43*, 256–263. [CrossRef]
44. Karimi, P. *Evaluating of Arsenic Adsorption from the Aqueous Solutions Using Porous Nanostructures*; University of Birjand: Birjand, Iran, 2018.



© 2019 by the authors. Licensee MDPI, Basel, Switzerland. This article is an open access article distributed under the terms and conditions of the Creative Commons Attribution (CC BY) license (http://creativecommons.org/licenses/by/4.0/).